Biochemical Society Transactions (2022) **50** 877–893
https://doi.org/10.1042/BST20190963

Review Article

Quinone binding sites of cyt *bc* complexes analysed by X-ray crystallography and cryogenic electron microscopy

Wei-Chun Kao[1] and **Carola Hunte**[1,2]

[1]Institute of Biochemistry and Molecular Biology, ZBMZ, Faculty of Medicine, University of Freiburg, Freiburg, Germany; [2]Signalling Research Centres BIOSS and CIBSS, University of Freiburg, Freiburg, Germany

Correspondence: Wei-Chun Kao (wei-chun.kao@biochemie.uni-freiburg.de) or Carola Hunte (carola.hunte@biochemie.uni-freiburg.de)

Cytochrome (cyt) bc_1, *bcc* and b_6f complexes, collectively referred to as cyt *bc* complexes, are homologous isoprenoid quinol oxidising enzymes present in diverse phylogenetic lineages. Cyt bc_1 and *bcc* complexes are constituents of the electron transport chain (ETC) of cellular respiration, and cyt b_6f complex is a component of the photosynthetic ETC. Cyt *bc* complexes share in general the same Mitchellian Q cycle mechanism, with which they accomplish proton translocation and thus contribute to the generation of proton motive force which drives ATP synthesis. They therefore require a quinol oxidation (Q_o) and a quinone reduction (Q_i) site. Yet, cyt *bc* complexes evolved to adapt to specific electrochemical properties of different quinone species and exhibit structural diversity. This review summarises structural information on native quinones and quinone-like inhibitors bound in cyt *bc* complexes resolved by X-ray crystallography and cryo-EM structures. Although the Q_i site architecture of cyt bc_1 complex and cyt *bcc* complex differs considerably, quinone molecules were resolved at the respective Q_i sites in very similar distance to haem b_H. In contrast, more diverse positions of native quinone molecules were resolved at Q_o sites, suggesting multiple quinone binding positions or captured snapshots of trajectories toward the catalytic site. A wide spectrum of inhibitors resolved at Q_o or Q_i site covers fungicides, antimalarial and antituberculosis medications and drug candidates. The impact of these structures for characterising the Q cycle mechanism, as well as their relevance for the development of medications and agrochemicals are discussed.

Introduction

Isoprenoid quinones are a family of natural electron and proton carriers present in prokaryotic cellular membranes, in the mitochondrial inner membrane and in the chloroplast thylakoid membrane [1–3]. The various isoprenoid quinone species differ in their water-soluble ring system and the length of the hydrophobic isoprenoid tails [4–6] (Figure 1A–E). The electrochemically active part of this family of molecules is the quinone ring system, which accepts two electrons and two protons to become the fully reduced quinol (Figure 1A), while the highly hydrophobic isoprenoid tail enhances its solubility in biological membranes. Isoprenoid quinone and quinol are substrates of respiratory chain and photosynthetic enzymes [7,8].

In the electron transport chain (ETC) of cellular respiration, NADH dehydrogenase (complex I) and succinate dehydrogenase (complex II) reduce quinone, harnessing the energy of redox equivalents obtained from metabolism while cytochrome bc_1 complex (cyt bc_1 complex, complex III) oxidises quinol and transfer the electrons to cytochrome *c* oxidase (cyt *c* oxidase, complex IV) via the electron carrier protein cytochrome (cyt) *c*. The cyt *c* oxidase catalyses the reduction in dioxygen to water. NADH dehydrogenase and cyt bc_1 complex couple quinone redox chemistry to proton translocation

Received: 5 January 2022
Revised: 6 March 2022
Accepted: 11 March 2022

Version of Record published: 31 March 2022

Biochemical Society Transactions (2022) **50** 877–893
https://doi.org/10.1042/BST20190963

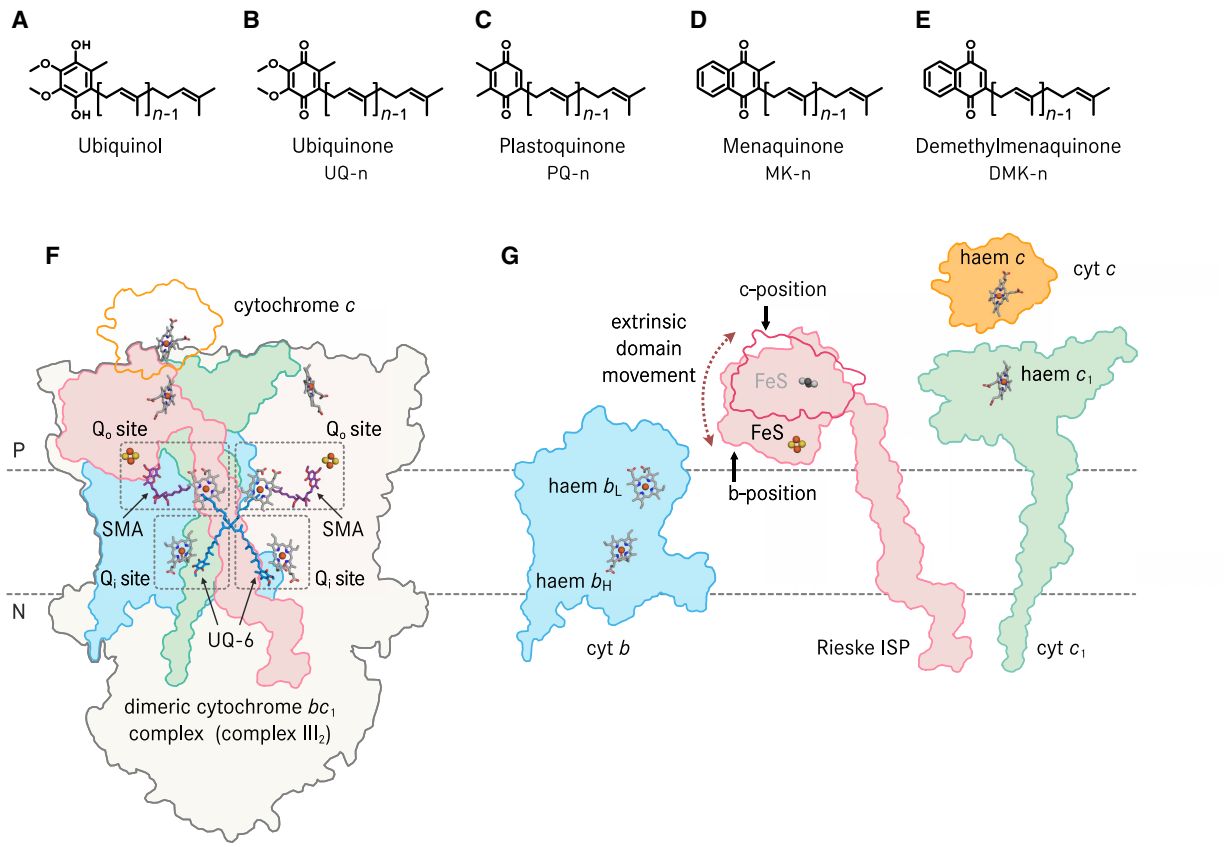

Figure 1. Cytochrome bc_1 complex and its substrates.

Chemical structures of (**A**) ubiquinol, (**B**) ubiquinone, (**C**) plastoquinone, (**D**) menaquinone and (**E**) demethylmenaquinone. The number of isoprenoid units is denoted as *n*. Ubiquinol is the reduced form of ubiquinone. (**F**) Cytochrome (cyt) bc_1 complex from *Saccharomyces cerevisiae* and its relative position in the inner mitochondrial membrane. The location of the quinol oxidation Q_o site is marked by the inhibitor stigmatellin (SMA) which was co-crystallised with cyt bc_1 complex (pdb 2ibz). The location of the quinone reduction Q_i site is indicated by ubiquinone-6 (UQ-6) which was co-isolated with the enzyme (pdb 2ibz). Soluble cyt *c* is a substrate of cyt bc_1 complex. Its docking position is illustrated based on the X-ray structure of the electron-transfer complex (pdb 3cx5). The three membrane-bound catalytic subunits of one protomer of the dimeric enzyme, namely cyt *b*, Rieske iron-sulfur protein (ISP) and cyt c_1 as well as the substrate cyt *c*, are separately illustrated in (**G**) The extrinsic domain of Rieske ISP undergoes diffusional movement and its position close to cyt *b* (b-position, pdb 2ibz) and close to cyt c_1 (c-position, pdb 1be3) are both indicated. The iron-sulfur cluster (FeS) is depicted in gray scale at the c-position and the extrinsic domain at the c-position is only outlined. P and N indicate the electropositive and -negative sides of the inner mitochondrial membrane. Iron atoms are depicted in brown, sulfur atoms are shown in yellow.

across the inner mitochondrial or bacterial cellular membrane to generate an electrochemical proton gradient and thereby power ATP synthesis [1,3]. In the ETC of photosynthesis, photosystem II utilises light energy to reduce quinone, and cyt b_6f complex [9–11], a homologue of cyt bc_1 complex, oxidises quinol and passes electrons to photosystem I. Photosystem II and cyt $b_6f$complex create a proton gradient across the chloroplast thylakoid membrane or the cyanobacterial plasma cellular membrane for ATP synthesis [12]. Therefore, cyt bc_1 and cyt b_6f complex are substantial contributors to the driving forces of cellular energy conversion.

Cyt bc_1 and cyt $b_6f$complexes form a large group of enzymes which all include a Rieske iron-sulfur protein (ISP), a *b*-type cytochrome (cyt *b or* cyt b_6-SUIV, 'subunit four') and a *c*-type cytochrome (cyt c_1, cyt *f* or di-haem cyt *cc*) as the core catalytic module (Figure 1F,G) [2,13,14]. Cyt bc_1 and cyt b_6f complexes are found in organisms from diverse phylogenetic clades [13], and they differ in composition in respect to number and types of peripheral subunits [10,15–17]. In actinobacteria, the catalytic Rieske ISP, cyt *b*, cyt *cc* and the cyt aa_3 oxidase plus peripheral subunits comprise the cyt *bcc-aa*$_3$ supercomplex [18,19]. Therefore, they are collectively referred to as cyt *bc* complexes in this mini-review.

In respiratory and photosynthetic ETCs, the overall forward reaction of cyt *bc* complexes is to oxidise quinol molecules and to reduce cytochrome *c* or plastocyanin, which will further transfer the electron to cyt *c* oxidase or photosystem I, respectively. Cyt *bc* complexes do not directly pump protons across the membrane such as for instance cyt *c* oxidases, instead, proton translocation is achieved through the Mitchellian Q cycle mechanism (Figure 2) [2,11,20–24]. As the first step in a Q cycle, a quinol molecule is oxidised at the quinol oxidation (Q_o) site of cyt *bc* complex close to the positive side (P-side) of the membrane (Figure 1F). Next, using the mitochondrial cyt bc_1 complex as an example, one electron of ubiquinol is transferred to the Rieske iron-sulfur cluster (FeS) and subsequently to haem c_1. The extrinsic domain of Rieske ISP undergoes a substantial conformational change [16,25–27] to bridge the 24 Å distance between the Q_o site quinol and haem c_1 (Figure 2).

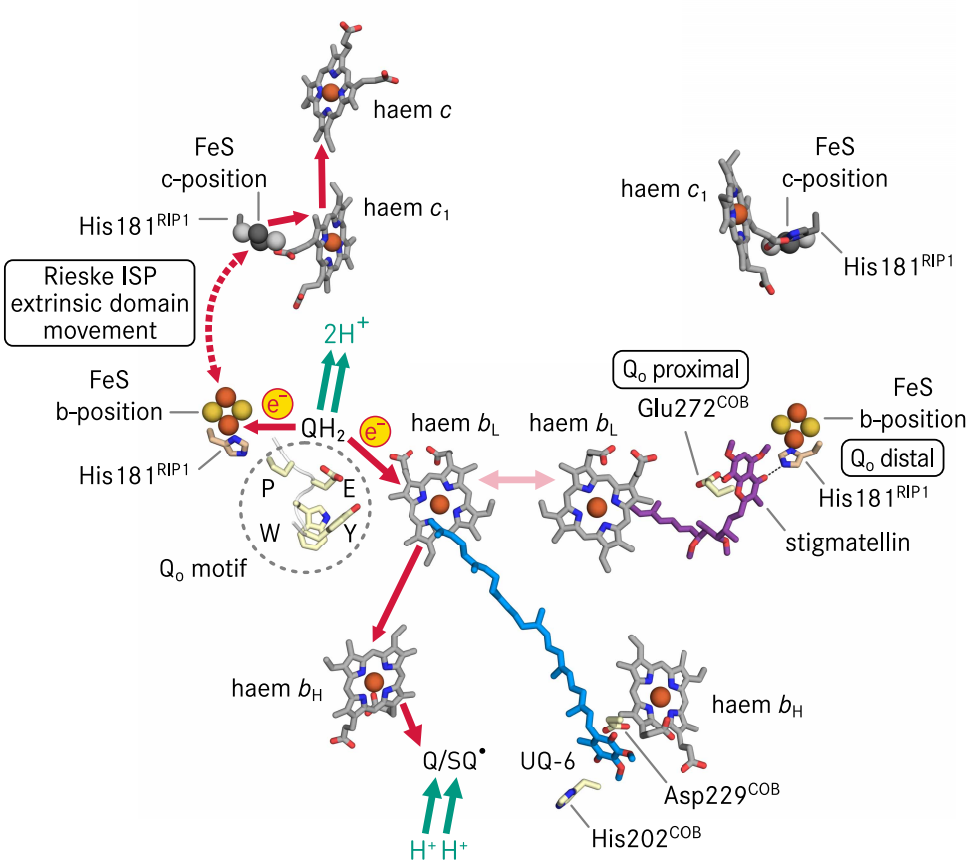

Figure 2. The Q cycle mechanism.

Catalytic centres of dimeric cyt bc_1 complex from *S. cerevisiae* are illustrated in two ways. The structure of the right half shows the inhibitor stigmatellin and the natural substrate UQ-6 in the X-ray structure (pdb 2ibz) as well as their hydrogen bonding partners. $His181^{RIP1}$ is also a ligand of the iron-sulfur cluster (FeS). Stigmatellin represents the position of a transition state of ubiquinol (QH_2) oxidation in the Q_o site, and UQ-6 indicates the position of ubiquinone/semiubiquinone ($Q/SQ^{\bullet}$) in the Q_i site. The structure of the left schematically shows the Q cycle mechanism. The four highly conserved residues of cyt *b* (COB): $Pro271^{COB}$ (P), $Glu272^{COB}$ (E), $Trp273^{COB}$ (W) and $Tyr274^{COB}$ (Y) in the Q_o site form the Q_o motif [14]. Electron transfer in cyt bc_1 complex can also cross the dimeric enzyme (pink arrow) [111]. Owing to the large-scale movement of the extrinsic domain (ED) of Rieske iron-sulfur protein (RIP1), the FeS is shown at two positions, the b-position (based on pdb 2ibz) close to the Q_o site quinol and the c-position close to haem c_1 (based on pdb 1be3). Whereas the Q_o site ubiquinol releases two electrons and two protons upon oxidation, only one electron is transferred to Q_i site, therefore the full reduction in the Q_i site quinone requires oxidation of a second ubiquinol molecule at the Q_o site and the uptake of two protons. The exact sequence of protonation steps at the Q_i site is not differentiated in this simplified scheme. Iron atoms are depicted in brown, sulfur atoms are shown in yellow. The FeS and its ligand $His181^{RIP1}$ at the c-position are shown in gray scale. Hydrogen bonds are depicted as dashed lines. Electron transfer pathways are shown in red, and proton release and uptake routes are in green.

Biochemical Society Transactions (2022) 50 877–893
https://doi.org/10.1042/BST20190963

Physiological electron transfer rates typically require a maximal distance of 14 Å between electron donor and acceptor [28,29]. The other electron is routed through the low potential haem b_L, the high potential haem b_H and reduces a quinone molecule in the Q_i site to a semiquinone radical ($SQ^{\bullet}$). In this process, the Q_o site quinol releases two protons to the P-side of the membrane and the complete reduction and protonation of a quinone molecule in the Q_i site needs oxidation of a second quinol at the Q_o site and proton uptake from the N-side of the membrane. Consequently, bifurcated electron transfer must be achieved upon quinol oxidation to enable the Q cycle, i.e. the highly reactive $SQ^{\bullet}$ at the Q_o site must be controlled to avoid short circuits [2,29–34] which lead to futile bypass reactions which would lower the efficiency of cellular respiration and can generate reactive oxygen species [29] that can cause oxidative damage to the cell [35].

Experimental structures of cyt *bc* complexes are essential to understand the molecular basis for efficient and safe electron and proton transfer mechanisms at Q_o and Q_i site. Position, geometry and distance of electron donors and acceptors, of substrate and analogous molecules as well as of prosthetic groups, are important to define electron transfer pathways [28]. Resolved positions of protonable amino acid side chains, hydronium ions (H_3O^+) or water molecules enable to identify proton transfer pathways [36]. Owing to the central role of cyt *bc* complexes in cellular respiration and in photosynthesis, structural biology studies of these complexes based on X-ray crystallography and cryogenic electron microscopy (cryo-EM) have delivered, over the years, a great number of experimental structures of mitochondrial cyt bc_1 complexes [16,17,37–40] as well as of respiratory supercomplexes [41–48], alpha-proteobacterial cyt bc_1 complexes [27,49,50], cyanobacterial [9] and chloroplast [10,51] cyt b_6f complexes and actinobacterial cyt *bcc-aa*$_3$ supercomplexes [19,52–54]. One should note that, the electrochemical properties of the redox-active centres of cyt *bc* complexes co-evolved with those of their native quinone substrates [13,55–57]. Hence, comparison of structures of cyt *bc* complexes with bound substrates sampled from a wide spectrum of organisms sheds light on the conserved structural basis of the Q cycle's quinone catalysis as well as on adaptations reflecting its molecular evolution, and may support development of medications precisely targeting different pathogens.

Quinone binding positions at the Q_o site

In cyt bc_1 and b_6f complexes, the Q_o site is embedded in subunit cyt *b* and at the interface with the mobile extrinsic domain of Rieske ISP (Figs. 1F, 2). The native substrate at the Q_o site is quinol, the reduced form of quinone, and the oxidised reaction product quinone has to leave the catalytic position at the Q_o site. So far, native quinone or quinol molecules were not resolved at the catalytic Q_o site position in X-ray crystallography studies (Table 1), in particular because crystal formation requires a defined conformation of the complex, and the unrestrained motion of the extrinsic domain of Rieske ISP may hinder this process. Consequently, the characterisation of the binding mode of the substrate in the Q_o site was supported by the use of inhibitors, and three binding positions at the Q_o site were suggested [58]. The proximal position (Figure 2) was assigned with myxothiazol, which is hydrogen-bonded solely to Glu272 of cyt *b* ($Glu272^{COB}$, yeast numbering) and shows no interaction to Rieske ISP [37]. The distal binding position (Figure 2) is exemplified by HHDBT, which is hydrogen-bonded to the iron-sulfur-cluster (FeS) ligand ($His181^{RIP1}$) of the Rieske protein, and to $Glu272^{COB}$ with a water-mediated hydrogen bond [59]. The third binding position is characterised with stigmatellin, which is hydrogen bonded directly to both $Glu272^{COB}$ and $His181^{RIP1}$ [17] (Figure 2). Stigmatellin also binds at the Q_o site of the cyt *bcc-aa*$_3$ supercomplex of *Corynebacterium glutamicum* in a similar manner as in the mitochondrial cyt bc_1 complexes [19], therefore it exhibits a conserved binding pose in the Q_o sites of cyt *bc* complexes which oxidise respectively ubiquinone or menaquinone. The Q_o site pocket is unlikely to accommodate two isoprenoid quinol molecules simultaneously due to spatial constraints, thus these aforementioned three inhibitor binding positions may reflect the locations of reaction intermediates in different oxidation or protonation states, as well as their interactions with potential proton acceptors [22,60,61]. One of the proton acceptors is $His181^{RIP1}$, which undergoes a pK_a change dependent on the Rieske protein redox state [62,63]. The other hypothetical proton acceptor is $Glu272^{COB}$. Its substitution with other residues by mutagenesis partially compromises the turnover of the enzyme [14] but its exact function remains elusive. $Glu272^{COB}$ is the second residue of the Q_o motif of cyt *b*, a highly conserved motif of four consecutive amino acid residues (Figure 2) present in all cyt *bc* complexes with systematic phylogenetic variations (PEWY in mitochondrial cyt *b*) [14]. The type of residue at the second position of the Q_o motif is correlated with the redox midpoint potential of cyt *bc* complex cofactors as well as with the quinone species [14]. Substrate binding positions in experimental structures of cyt *bc* complexes from different organisms would be very important to derive the conserved structural basis of catalysis as well as species-specific adaptations.

Table 1 Structures of cyt *bc* complexes with bound native quinone molecule resolved

Position			Year	Complex type	pdb	Res (Å)	Method	Origin	Quinone
	Q_i		1998	cyt bc_1 complex	1bcc	3.16	X-ray	*Gallus gallus*	UQ-10
	Q_i		2000	cyt bc_1 complex	1ezv	2.30	X-ray	*Saccharomyces cerevisiae*	UQ-6
	Q_i		2003	cyt b_6f complex	1vf5	3.00	X-ray	*Mastigocladus laminosus*	PQ-9
	Q_i		2005	cyt bc_1 complex	1pp9	2.10	X-ray	*Bos taurus*	UQ-10
	Q_i		2008	cyt bc_1 complex	2qjy	2.40	X-ray	*Rhodobacter sphaeroides*	UQ-10
Q_o	Q_i		2018	Supercomplex III_2/IV_2	6adq	3.50	cryo-EM	*Mycobacterium smegmatis*	MK-9
Q_o	Q_i		2018	Supercomplex III_2/IV_2	6hwh	3.30	cryo-EM	*Mycobacterium smegmatis*	MK-9
Q_o	Q_i		2019	Supercomplex I/III_2	6q9e	3.90	cryo-EM	*Ovis aries*	UQ-10
Q_o	Q_i		2019	cyt b_6f complex	6rqf	3.60	cryo-EM	*Spinacia oleracea*	PQ-9
	Q_i		2019	Supercomplex III_2/IV	6giq	3.23	cryo-EM	*Saccharomyces cerevisiae*	UQ-6
	Q_i		2019	Supercomplex III_2/IV_2	6hu9	3.35	cryo-EM	*Saccharomyces cerevisiae*	UQ-6
	Q_i		2020	cyt bc_1 complex	6kls	3.30	cryo-EM	*Aquifex aeolicus*	DMK-7
Q_o	Q_i		2021	cyt bc_1 complex	7rja	3.00	cryo-EM	*Candida albicans*	UQ-10
Q_o	Q_i		2021	Supercomplex III_2/IV_2	7e1v	2.68	cryo-EM	*Mycobacterium tuberculosis/smegmatis*	MK-9
Q_o	Q_i	Q_c	2021	Supercomplex III_2/IV_2	7q21	2.90	cryo-EM	*Corynebacterium glutamicum*	MK-9
	Q_i	Q_c	2022	Supercomplex III_2/IV_2	7qhm	2.80	cryo-EM	*Corynebacterium glutamicum*	MK-9
Q_o	Q_i	Q_c	2022	Supercomplex III_2/IV_2	7qho	3.10	cryo-EM	*Corynebacterium glutamicum*	MK-9

Binding position was assigned according to authors' descriptions in the original publications (see text for references). The pdb code, resolution (Res) and experimental method of each entry are sourced from RCSB PDB (https://www.rcsb.org).

Recently, native co-isolated quinone molecules at or in proximity to the Q_o site were identified in several cryo-EM structures of respiratory chain supercomplexes (Table 1). In a mammalian respiratory I/III_2 supercomplex [48], which is composed of a NADH dehydrogenase (complex I) and a dimeric cyt bc_1 complex (complex III_2), an ubiquinone molecule was identified in the Q_o site which is distal to complex I, whereas the Q_o site proximal to the quinone reduction tunnel of complex I was unoccupied (Figure 3A). The authors proposed that the Q_o site close to complex I would accept ubiquinol reduced by complex I as they share the shortest diffusion distance [48]. The cryo-EM structure of cyt bc_1 complex from *Candida albicans* contains a ubiquinone molecule in the Q_o site of both protomers [40] (Figure 3B). By superimposition of the mammalian supercomplex I/III_2 with *Candida albicans* complex III, and yeast cyt bc_1 complex co-crystallised with stigmatellin, a trajectory of Q_o site occupants can be deduced (Figure 3C). In comparison, stigmatellin reached deepest into the Q_o site pocket. The ubiquinone molecules resolved in the cryo-EM structures only partially overlap with the stigmatellin binding position. Concomitantly, the FeS cluster of the cryo-EM structures are further apart from the Q_o site. The FeS of the yeast cyt bc_1 complex is located at the closest distance to the Q_o site, as it is constrained by a hydrogen bond from its own ligand $His181^{RIP1}$ to stigmatellin (Figure 2). In contrast, the FeS clusters of the mammalian supercomplex I/III_2 and the *Candida albicans* complex III are more distant from the Q_o site. The distances between ubiquinone and the FeS histidine ligand in these two complexes are larger than 4.5 Å, which is too long for a hydrogen bond. These two positions in the cryo-EM structures likely represent the states of ubiquinone, the product of ubiquinol-oxidation, exiting the catalytic Q_o site position.

In prokaryotes, a co-isolated menaquinone at the Q_o site was resolved in two cryo-EM structure of *bcc-aa*$_3$ supercomplex from the actinobacterium *Corynebacterium glutamicum* [19,54] (Figure 4A). This menaquinone molecule is positioned in ∼6 Å distance to the closest possible H-bonding partners $His355^{QcrA}$ and $Tyr153^{QcrB}$, respectively (QcrA and QcrB are homologous to mitochondrial Rieske ISP and cyt *b*), and is 9.4 and 13.7 Å apart from FeS and haem b_L, respectively [19]. In a cryo-EM structure of the actinobacterial cyt *bcc-aa*$_3$ supercomplex from *Mycobacterium smegmatis*, a menaquinone molecule was described in 14 Å and 16 Å distance from FeS and haem b_L, respectively (Figure 4B) [52]. This binding position agrees with a menaquinone molecule resolved in another *M. smegmatis* cryo-EM structure [64], as well as a menaquinone molecule identified

Biochemical Society Transactions (2022) **50** 877–893
https://doi.org/10.1042/BST20190963

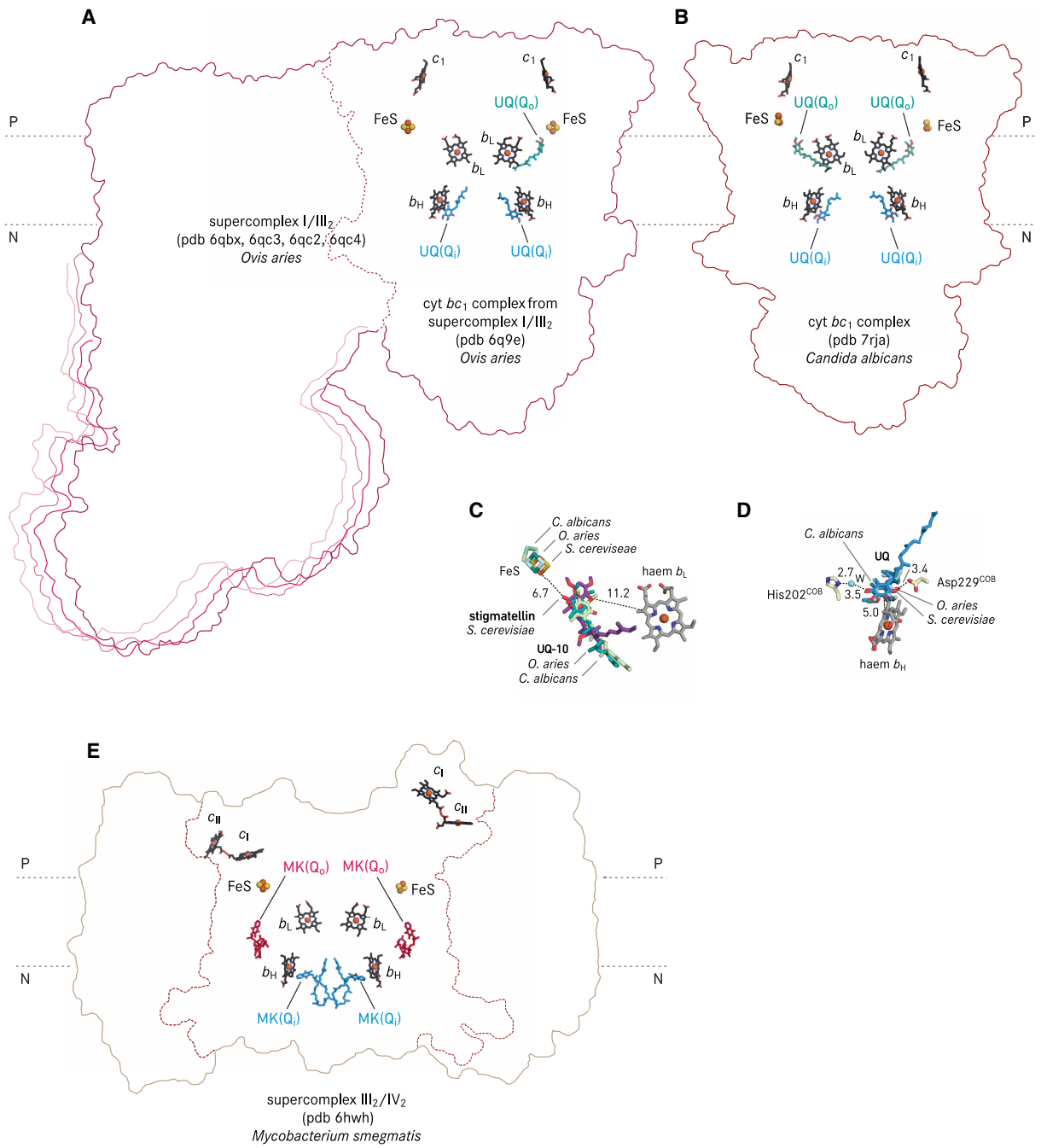

Figure 3. Positions of natural quinone molecules resolved in supercomplex I/III$_2$, cyt *bc*$_1$ complex and cyt *bcc-aa*$_3$ supercomplex. Part 1 of 2 (**A**) cryo-EM structure of cyt *bc*$_1$ complex as part of the supercomplex I/III$_2$ from sheep. The cryo-EM map of cyt *bc*$_1$ complex was reconstructed from focused-refinement of four supercomplex I/III$_2$ maps representing different conformational states [48], therefore the outlines of all four corresponding supercomplex structures were all illustrated. Co-ordinates of supercomplex I/III$_2$ were superposed on one cyt *b* of pdb 6q9e using secondary structure maching in Coot [112]. (**B**) cryo-EM structure of cyt *bc*$_1$ complex from *Candida albicans* [40]. (**C**) Comparison of stigmatellin and ubiquinone-10 (UQ-10) binding positions by superimposition of the co-ordinates of the cyt *bc*$_1$ complex structure. Cyt *b* of the yeast (*S. cerevisiae*) cyt *bc*$_1$ complex (pdb 2ibz, with stigmatellin [67]) was used as reference, and cyt *b* of pdb 6q9e (*O. aries*), and pdb 7rja (*C. albicans*) were superposed using secondary structure matching in Coot [112]. The FeS of all structures are shown, whereas only the haem *b*$_L$ of pdb 2ibz is displayed for the sake of clarity. All distances are in Å. (**D**) Comparison of ubiquinone binding positions at the Q$_i$ site. Water molecule is labelled as W. Haem *b*$_H$ and the side chains of Asp229^{COB}, His202^{COB} are from pdb 2ibz. (**E**) cryo-EM structure of cyt *bcc-aa*$_3$ supercomplex (supercomplex

Figure 3. Positions of natural quinone molecules resolved in supercomplex I/III$_2$, cyt *bc*$_1$ complex and cyt *bcc-aa*$_3$ supercomplex. Part 2 of 2

III$_2$/IV$_2$) from *Mycobacterium smegmatis* (pdb 6hwh) [53]. For Figures 3–5, all the quinone types and locations are assigned according to the positions reported in the original publications. For cyt *bc* complexes resolved within a supercomplex, the boundary of the cyt *bc* complex is depicted in dashed lines, and only prosthetic groups of cyt *bc* complexes are shown. The electropositive and -negative sides of the membrane are indicated with P and N, respectively. Depending on the resolution and data quality, the isoprenoid units of quinones structurally resolved can deviate from the full length of native isoprenoid quinones of the given species.

in the hybrid supercomplex composed of the *M. tuberculosis* cyt *bcc* complex and *M. smegmatis* cyt *aa*$_3$ oxidase [65] (Figure 4C). By superimposition of the structures of the corynebacterial supercomplex with stigmatellin [19], with menaquinone [19,54], and the mycobacterial supercomplex structures with menaquinone [52,64,65], genus-specific consensus menaquinone binding positions can be deduced (Figure 4D). The locations of FeS in these structures are static. The menaquinone molecules in the two structures of the corynebacterial supercomplex both partially overlap with the stigmatellin binding position, whereas the menaquinone molecules of the three structures of the mycobacterial supercomplex were consistently located closer to the entrance of the quinone exchange cavity (Figure 4D). These experimentally resolved menaquinone molecules likely illustrate a migration path to the catalytic position of menaquinol, which is represented by the transition state analogue stigmatellin [66,67]. Interestingly, the Q$_o$ site menaquinone position assigned in a *M. smegmatis* supercomplex (pdb 6hwh, Figure 3D) [53] does not agree with the Q$_o$ site menaquinone positions shown in other four actinobacterial supercomplex structures and its naphthoquinone ring was resolved in 21 Å and 19 Å to FeS and the haem b_L iron [53], therefore this model is not included in Figure 4D.

In addition to ubiquinone and menaquinone at the Q$_o$ site, a plastoquinone was described in the cryo-EM structure of cyt b_6f complex from spinach chloroplasts [51], with its benzoquinone ring 26.4 Å apart from FeS and 16.2 Å from haem b_L. It was described as in an approaching position to the Q$_o$ site (Figure 5A). Moreover, the entrance of the Q$_o$ site in this structure is partially blocked by the phytyl tail of chlorophyll (Chl), which was suggested to gate the Q$_o$ site access [51].

Although quinone molecules were resolved in the Q$_o$ site of cyt *bc* complexes in several positions, structural information of the natural substrate in the catalytic relevant position in the Q$_o$ site with close distance to electron and proton acceptors is still lacking. So far, only the structures with inhibitors bound at the Q$_o$ site suggest the potential proton acceptors for quinol oxidation. Taken together, the cryo-EM structure of the ovine supercomplex I/III$_2$ provided a first hint of a co-isolated quinone in the Q$_o$ pocket in the context of substrate exchange between complexes I and III. The diverse binding positions of native co-purified ubiquinone, menaquinone and plastoquinone molecules resolved in structures of cyt *bc* complexes, most likely exemplify snapshots of their migration paths in and out of the active site and stand-by positions.

Quinone binding positions at the Q$_i$ site

In contrast with the Q$_o$ site characterisation, many X-ray and cryo-EM structures of cyt *bc* complexes described co-purified quinone molecules in the Q$_i$ site. A plausible explanation is that the Q$_i$ site substrate has to be stabilised within the cyt *b* pocket to ensure a full Q cycle turnover with the two-step reduction to semiquinone and quinol, which is strictly coupled to the oxidation of two quinol molecules in the Q$_o$ site (Figure 2). Binding poses of Q$_i$ site ubiquinone including ordered water molecules were obtained with high resolution X-ray structures of bovine [38], chicken [39,68], yeast cyt *bc*$_1$ complexes (Figure 5D) [17] and that from *Rhodobacter sphaeroides* (Figure 5B) [69]. In brief, the Q$_i$ site ubiquinone is consistently located within ca. 5 Å distance to the porphyrin ring of haem b_H (Figure 3D) in the different structures. Two proposed proton transfer pathways were assigned from the protein surface on the mitochondrial matrix side (the electro-negative side) to Asp229^{COB} and His202^{COB} (yeast numbering, Figs. 2, 3D). Each residue is connected via hydrogen bonds to a carbonyl group of the Q$_i$ site ubiquinone. The exact hydrogen bond pattern, whether it is a direct interaction or mediated by water molecules, varies in X-ray structures of the complex from different species [21]. That the binding of the Q$_i$ site inhibitor antimycin A replaced the natively occupied ubiquinone with Asp229^{COB} as its direct interaction partner (in the bovine structure, pdb 1ppj) [38].

X-ray crystallographic analysis resolved highly ordered quinone molecules in the Q$_i$ site of crystallised cyt *bc*$_1$ complex. The power of cryo-EM to better cope with global or local protein dynamics brought forward a higher

Biochemical Society Transactions (2022) **50** 877–893
https://doi.org/10.1042/BST20190963

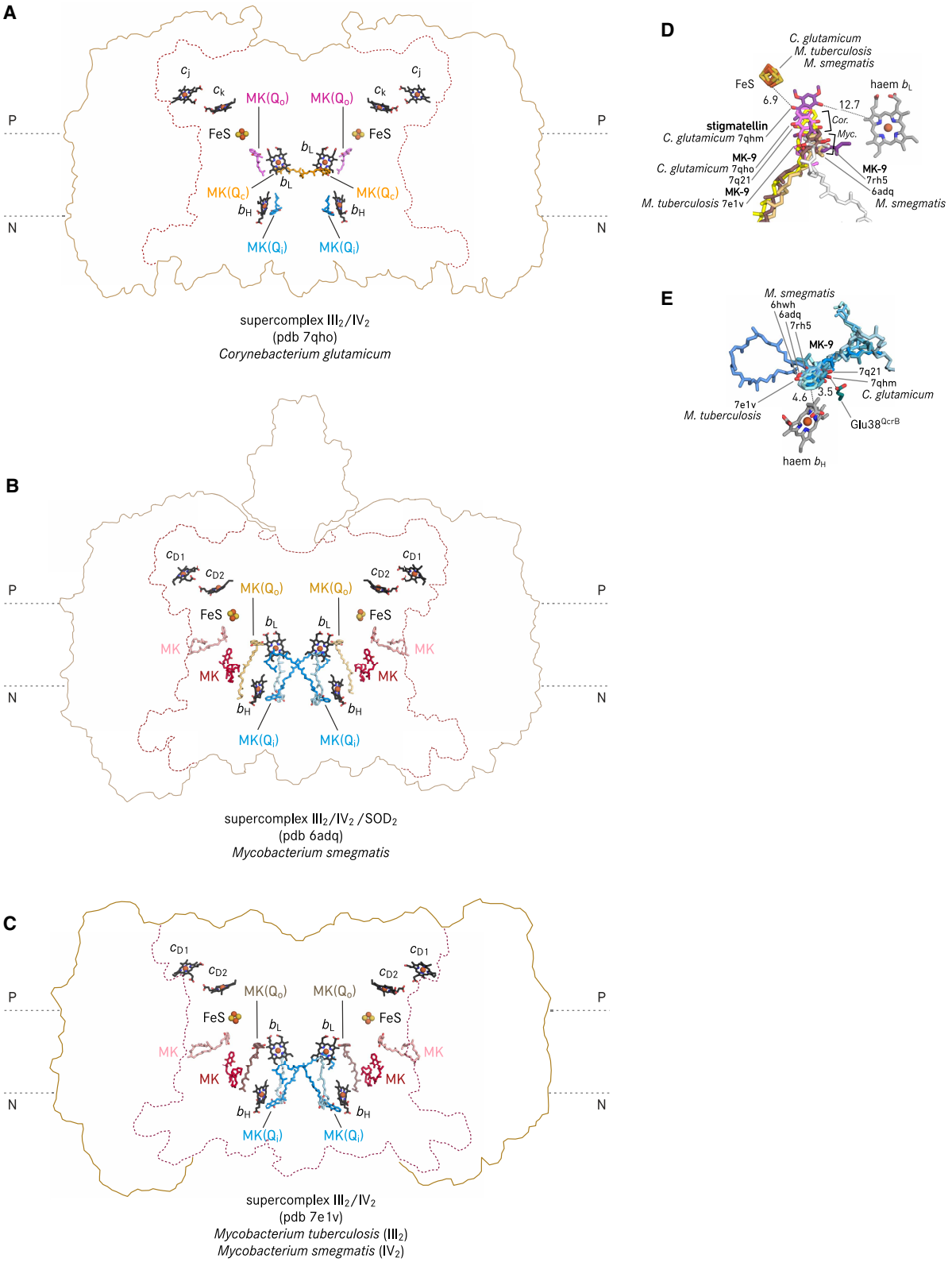

Figure 4. Positions of natural quinone molecules resolved in cyt *bcc-aa*$_3$ supercomplex. Part 1 of 2

(**A**) cryo-EM structure of cyt *bcc-aa*$_3$ supercomplex (supercomplex III_2/IV_2) from *Corynebacterium glutamicum* [19]. (**B**) cryo-EM structure of cyt *bcc-aa*$_3$ supercomplex (supercomplex $III_2/IV_2/SOD_2$) from *Mycobacterium smegmatis* [52]. (**C**) cryo-EM structure

Figure 4. Positions of natural quinone molecules resolved in cyt *bcc-aa*$_3$ supercomplex. Part 2 of 2

of a hybrid cyt *bcc-aa*$_3$ supercomplex (supercomplex III_2/IV_2) with complex III_2 from *M. tuberculosis* and complex IV_2 from *M. smegmatis* [65]. (**D**) Comparison of stigmatellin and menaquinone-9 (MK-9) binding positions by superimpositioning the co-ordinates of cyt *bcc-aa*$_3$ supercomplex. The QcrB of the *C. glutamicum* cyt *bcc-aa*$_3$ supercomplex (pdb 7qhm, with stigmatellin) was used as the reference, and the QcrB of pdb 7qho (*C. glutamicum*), pdb 7q21 (*C. glutamicum*), pdb 6adq (*M. smegmatis*), pdb 7rh5 (*M. smegmatis*), and pdb 7e1v (*M. tuberculosis*) were superposed using secondary structure matching in Coot [112]. The FeS of all structures are shown, whereas only the haem b_L of pdb 7q21is displayed for the sake of clarity. *Cor*. and *Myc*, respectively, indicate the consensus position of the naphthoquinone ring of MK-9 in the corynebacterial and mycobacterial structures. (**E**) Comparison of MK-9 resolved in the Q_i site. The $Glu38^{QcrB}$ side chain and haem b_H are from pdb 7qhm. All distances are in Å.

variety of quinone binding modes at the Q_i site. In cryo-EM structures of mitochondrial respiratory chain supercomplexes, of the yeast supercomplex III_2/IV [47] (Figure 5E) and the ovine supercomplex I/III_2 [48] (Figure 3A) one ubiquinone molecule was resolved in each Q_i site, in a position consistent to the known binding poses in X-ray structures of mitochondrial cyt bc_1 complexes (Figs. 3D, 5D). In contrast, in the cryo-EM structure of yeast supercomplex III_2/IV_2 [46], an ubiquinone ring was modelled on the internal two-fold symmetry axis of the dimeric cyt bc_1 complex with two alternate conformations (Figure 5F). The distance from the quinone ring to haem b_H of each protomer is 15.3 Å.

In actinobacterial respiratory supercomplexes, a menaquinone molecule was identified in the Q_i site of the cyt *bcc-aa*$_3$ supercomplex of *C. glutamicum*, *M. smegmatis*, and *M. tuberculosis* (Figs. 3E, 4A–C) [19,52–54,65]. The interaction mode between haem b_H and menaquinone is very similar to that of ubiquinone in cyt bc_1 complexes (Figure 3D). In contrast with mitochondrial cyt bc_1 complexes, in which protons could be delivered to the Q_i site ubiquinone via a histidine and an aspartate residue, of which the side chains have direct or water-mediated hydrogen bonds to both carbonyl groups of the quinone, the menaquinone molecule resolved in the Q_i site of the cyt *bcc* complex from *C. glutamicum* is single hydrogen-bonded directly to a glutamate side chain (Figure 4E) [19]. Interestingly, a second menaquinone was identified near the Q_i site of the *bcc* complex from *M. smegmatis* [52], with its naphthoquinone ring in 3.6 Å distance to that of the other menaquinone in the Q_i site (Figure 4B). This short distance between the two menaquinone molecules in and close to the Q_i site would allow a consecutive reduction from one to the other. Menaquinone and ubiquinone are quinone species of low (−78 mV) and high (+90 mV) redox midpoint potential, respectively [13,14,55–57]. The hyperthermophilic *Aquifex aeolicus* uses demethylmenaquinone (DMK) which has a potential of +36 mV [70], giving it a transitional position in the evolution of cyt *bc* complexes from low to high potentials [71]. The cryo-EM structure of the *A. aeolicus* cyt bc_1 complex with bound DMK molecules at the Q_i site (Figure 5C) revealed a 6.1 Å distance from the naphthoquinone ring to haem b_H [72], which is in good agreement with the binding mode of the Q_i site ubiquinone in yeast and *Rhodobacter* homologues as well as the Q_i site menaquinone of the actinobacterial cyt *bcc-aa*$_3$ supercomplex.

The most unique Q_i site architecture of cyt *bc* complexes is found in cyt b_6f complexes. The position equivalent to the aforementioned ubiquinone and menaquinone ring plane in the Q_i site is replaced by a high spin *c*-type haem (haem c_i), which is attached via a single thioether bond to cyt b_6 and which has no amino acid axial ligand [9,10]. A recent cryo-EM structure of spinach cyt b_6f complex revealed the position of a plastoquinone molecule at the Q_i site (Figure 5A) [51]. The benzoquinone ring of this plastoquinone molecule is 4.4 Å apart from the haem c_i porphyrin ring. In addition, one of its carbonyl groups is hydrogen-bonded to a propionate carboxylate of haem c_i in 3.2 Å. Notably, the Q_i site plastoquinone breaks the internal two-fold symmetry of cyt b_6f complex (Figure 5A). The isoprenoid tail of the Q_i site plastoquinone extends into the entrance of the unoccupied Q_i site of the other protomer while a second plastoquinone was modelled in a diagonal position with respect to the Q_i site plastoquinone, in a position approaching the Q_o site of the other protomer [51]. In addition, the Q_i site occupancy of plastoquinone seems to be correlated to the orientation of the propionate group of haem c_i, which may control access to a potential proton transfer pathway from the stromal side (the electronegative side) via Asp20 and Arg207 [51]. It was therefore hypothesised that both Q_i sites are not simultaneously functional [51].

Whereas high-resolution X-ray structures revealed detailed binding modes of the Q_i site ubiquinone in mitochondrial cyt bc_1 complexes, cryo-EM structures more recently provided additional information of ubiquinone positions in the context of supercomplexes, and previously unavailable structures of plastoquinone and

Biochemical Society Transactions (2022) **50** 877–893
https://doi.org/10.1042/BST20190963

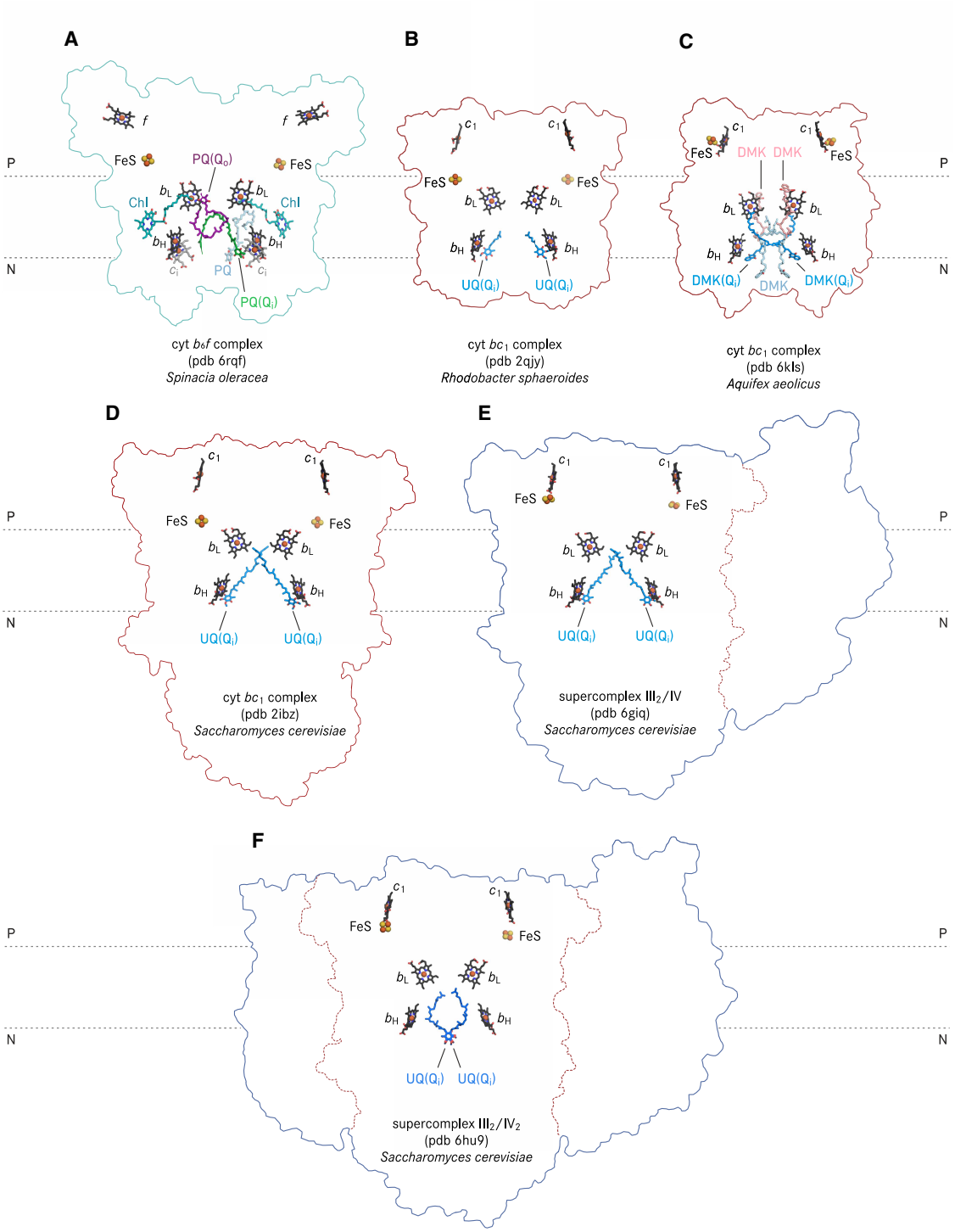

Figure 5. Positions of natural quinone molecules resolved in cyt b_6f and bc_1 complexes. Part 1 of 2

(**A**) cryo-EM structure of cyt b_6f complex (pdb 6rqf) from spinach [51]. (**B**) X-ray structure of cyt bc_1 complex (pdb 2qjy) from *Rhodobacter sphaeroides* [69]; (**C**) cryo-EM structure of cyt bc_1 complex (pdb 6kls) from *Aquifex aeolicus* [72]; (**D**) X-ray structure of cyt bc_1 complex (pdb 2ibz) from baker's yeast [67]. The deposited structure contains only one protomer which belongs to the crystallographic asymmetric unit. Here the dimeric structure shown was generated by applying symmetry operation; (**E**) cryo-EM structure of a supercomplex containing a dimeric cyt bc_1 complex and a monomeric cyt *c* oxidase

Figure 5. Positions of natural quinone molecules resolved in cyt b_6f and bc_1 complexes. Part 2 of 2

(supercomplex III_2/IV, pdb 6giq) from baker's yeast [47]; (**F**) cryo-EM structure of a supercomplex containing a dimeric cyt bc_1 complex and a dimeric cyt *c* oxidase (supercomplex III_2/IV_2, pdb 6hu9) from baker's yeast [46].

menaquinone-occupied Q_i sites which show considerably different architecture as compared with mitochondria cyt bc_1 complexes. We anticipate that alternate reaction mechanisms will be required to accomplish quinone reduction and protonation at the Q_i site in these complexes.

Inhibitors bound at Q_o or Q_i site of cyt *bc* complexes

The use of Q_o and Q_i site inhibitors was instrumental in studies of cyt bc_1 complexes in order to explore the molecular basis of the Q cycle mechanism and to elucidate electron transfer pathways [58]. Their binding positions in Q_o and Q_i site, in particular that of stigmatellin [16,17], myxothiazol, UHDBT, NQNO and antimycin A [37] were all analyzed as early as the first X-ray structures of cyt bc_1 complexes were determined (Table 2). Stigmatellin is a semiquinone analogue, i.e. it mimics a transition state of quinol oxidation and reduction [66,67], which is difficult to be captured in protein crystals or cryo-EM specimens with natural substrates. Therefore, its binding poses in the Q_o site of cyt bc_1 complex [17] and cyt *bcc* complex [19] provide insights in the catalytic position from which the protons and electrons are released to their respective acceptors. Parallel to fundamental research, cyt bc_1 complex inhibitors are also of great agricultural and medical importance: Azoxystrobin [37,73] belongs to the strobilurins [74], a group of chemically similar compounds [75] which accounted for 27% of the total fungicide worldwide sales in year 2015 [76]. The Q_o site inhibitor Famoxadone is a fungicide for crops [77]. Atovaquone [78] is used in a fixed-dose combination with proguanil as antimalarial drug [79–81], and is also used for treating pneumocystis infection [82]. Note that both, atovaquone and strobilurin inhibitors target the Q_o site, however, resistances were identified soon after these compounds were made commercially available [81,83–85]. Consequently, development of cyt bc_1 complex inhibitors targeting the Q_i site could provide a chance to bypass this issue [86,87]. Interestingly, in the past 5 years, almost all new antimalarial drug candidates resolved in structures of cyt bc_1 complexes published in the RCSB protein data bank (PDB, www.rcsb.org) are Q_i site inhibitors (Table 2). This includes the X-ray structures of cyt bc_1 complex inhibited by the antimalarial 4(1H)-pyridones GSK 932121 and GW844520 [88], MJM170 [89], and a 2-pyrazolyl quinolone WDH2G7 [90]. Although X-ray structures can deliver information on protein–ligand interaction with atomic detail, structure-based drug discovery is often hindered by the amount of protein available, time required for crystallisation trials, and conformational heterogeneity or dynamic properties of proteins. The cryo-EM structures of cyt bc_1 complex with bound compounds SCR0911 and GSK 932121 [91] exemplified the scope of cryo-EM structures to characterise binding of drug candidates to target proteins with dynamic properties. Cryo-EM structures of the *Mycobacterium* cyt *bcc-aa*$_3$ complex with the tuberculosis drug candidate telacebec (Q203) [92] and with TB47 bound at the Q_o site demonstrated this approach for bacterial cyt *bc* complexes and supercomplexes [64,65]. Cryo-EM has the advantage of lower sample consumption for single particle analysis as compared with X-ray crystallography. This is especially important for proteins isolated from scarce sources such as patient tissue [93], or from pathogens which are difficult or dangerous to cultivate [94]. In this respect, cryo-EM also opens new possibilities in obtaining structural information of cyt *bc* complexes to develop novel human medications as well as agrochemicals [95–98].

Detergent, lipids and the native membrane

Owing to the nature that membrane proteins are located in the lipidic compartments of the cell [99], structural biology studies of membrane proteins have greatly benefited from the use of detergents to solubilise them from their native environment into aqueous solution. Detergent molecules bind to hydrophobic surfaces of membrane proteins and increase their solubility in aqueous environment. Detergents differ in their chemical and physical properties and the selection of the type of detergent is key to prepare well-diffracting membrane protein crystals [100] as well as cryo-EM grids with good contrast and particle distributions [101]. However, detergents compete with the binding of lipids and lipidic compounds such as quinone thus delipidation is unavoidable. Severe delipidation compromises the stability and eventually the integrity of isolated membrane proteins, which may cause artificial structural disorder and may account for poor resolution of X-ray and cryo-EM structures. Reintroducing the detergent solubilised membrane protein back into lipidic cubic phase

Biochemical Society Transactions (2022) **50** 877–893
https://doi.org/10.1042/BST20190963

Table 2. Structures of cyt *bc* complexes with bound non-native compounds and their application Part 1 of 2

Position		Year	Non-native compound	pdb	Res (Å)	Method	Origin	Applications
	Q_i	1998	Antimycin	3bcc	3.70	X-ray	*Gallus gallus*	Research
Q_o		1998	Stigmatellin	3h1j	3.00	X-ray	*Gallus gallus*	Research
Q_o		2000	Stigmatellin	1ezv	2.30	X-ray	*Saccharomyces cerevisiae*	Research
Q_o		2003	Famoxadone	1l0l	2.35	X-ray	*Bos taurus*	Fungicide
Q_o	Q_i	2003	NQNO	1nu1	3.20	X-ray	*Bos taurus*	Research
Q_o		2003	Tridecylstigmatellin	1vf5	3.00	X-ray	*Mastigocladus laminosus*	Research
Q_o		2003	Tridecylstigmatellin	1q90	3.10	X-ray	*Clamydomonas reinhardtii*	Research
Q_o		2004	Azoxystrobin	1sqb	2.69	X-ray	*Bos taurus*	Fungicide
Q_o		2004	HHDBT	1p84	2.50	X-ray	*Saccharomyces cerevisiae*	Research
Q_o		2004	MOAS	1sqq	3.00	X-ray	*Bos taurus*	Fungicide
Q_o		2004	Myxothizol	1sqp	2.70	X-ray	*Bos taurus*	Research
Q_o		2004	UHDBT	1sqv	2.85	X-ray	*Bos taurus*	Research
	Q_i	2005	Antimycin A	1ppj	2.10	X-ray	*Bos taurus*	Research
Q_o		2005	Stigmatellin	1pp9	2.10	X-ray	*Bos taurus*	Research
Q_o		2006	JG144	2fyu	2.26	X-ray	*Bos taurus*	Fungicide
Q_o		2006	Stigmatellin	2fyn	3.20	X-ray	*Rhodobacter sphaeroides*	Research
Q_o		2007	NQNO	2e75	3.55	X-ray	*Mastigocladus laminosus*	Research
Q_o		2008	Crocacin-D iodinated analogue	3cwb	3.51	X-ray	*Gallus gallus*	Fungicide
Q_o		2008	Stigmatellin	2qjy	2.40	X-ray	*Rhodobacter sphaeroides*	Research
Q_o	Q_i	2010	Ascochlorin	3h1l	3.21	X-ray	*Gallus gallus*	Anti-Trypanosomiasis
Q_o		2010	Azoxystrobin	3l71	2.84	X-ray	*Gallus gallus*	Fungicide
Q_o		2010	Famoxadone	3l74	2.76	X-ray	*Gallus gallus*	Fungicide
Q_o		2010	Fenamidone	3l75	2.79	X-ray	*Gallus gallus*	Fungicide
Q_o		2010	Kresoxim-methyl	3l72	3.06	X-ray	*Gallus gallus*	Fungicide
Q_o		2010	Kresoxim-methyl iodinated derivative	3h1k	3.48	X-ray	*Gallus gallus*	Fungicide
Q_o		2010	Triazolone	3l73	3.04	X-ray	*Gallus gallus*	Fungicide
Q_o		2010	Trifloxystrobin	3l70	2.75	X-ray	*Gallus gallus*	Fungicide
Q_o		2011	Stigmatellin	2yiu	2.70	X-ray	*Paracoccus denitrificans*	Research
Q_o		2012	MOA-like (WF3)	3tgu	2.70	X-ray	*Gallus gallus*	Fungicide
Q_o		2014	Atovaquone	4pd4	3.04	X-ray	*Saccharomyces cerevisiae*	Antimalarial
	Q_i	2015	4(1H)-pyridone GSK932121	4d6u	4.09	X-ray	*Bos taurus*	Antimalarial
	Q_i	2015	4(1H)-pyridone GW844520	4d6t	3.57	X-ray	*Bos taurus*	Antimalarial
Q_o		2015	Famoxadone	5kkz	2.97	X-ray	*Rhodobacter sphaeroides*	Fungicide
Q_o		2015	MOA-like (Y52)	4u3f	3.23	X-ray	*Gallus gallus*	Fungicide
Q_o		2016	Fenamidone	5klv	2.65	X-ray	*Bos taurus*	Fungicide
	Q_i	2016	MJM170	5mni	3.50	X-ray	*Bos taurus*	Anti-Apicomplexan
	Q_i	2018	2-pyrazolyl quinolone WDH2G7	6haw	3.45	X-ray	*Bos taurus*	Antimalarial
	Q_i	2018	4(1H)-pyridone GSK932121	6fo0	4.10	cryo-EM	*Bos taurus*	Antimalarial
	Q_i	2018	SCR0911	5okd	3.10	X-ray	*Bos taurus*	Antimalarial
	Q_i	2018	SCR0911	6fo6	4.10	cryo-EM	*Bos taurus*	Antimalarial
Q_o		2019	Azoxystrobin	6nhh	3.00	X-ray	*Rhodobacter sphaeroides*	Fungicide
	Q_i	2020	Antimycin A	6klv	3.20	cryo-EM	*Aquifex aeolicus*	Research

Continued

Table 2. Structures of cyt *bc* complexes with bound non-native compounds and their application Part 2 of 2

Position	Year	Non-native compound	pdb	Res (Å)	Method	Origin	Applications
Q_o	2021	Telacebec (Q203)	7rh7	3.00	cryo-EM	*Mycobacterium smegmatis*	Anti-Tuberculosis
Q_o	2021	Telacebec (Q203)	7e1w	2.67	cryo-EM	*Mycobacterium tuberculosis/smegmatis*	Anti-Tuberculosis
Q_o	2021	TB47	7e1x	2.93	cryo-EM	*Mycobacterium tuberculosis/smegmatis*	Anti-Tuberculosis
Q_o	2021	Inz-5	7rje	3.30	cryo-EM	*Candida albicans*	Fungicide
Q_o	2022	Stigmatellin	7qhm	2.80	cryo-EM	*Corynebacterium glutamicum*	Research

This list is not exhaustive, only the first structure of a unique species containing a particular compound, or the structure resolved with the highest resolution are included. The pdb code, resolution (Res) and experimental method of each entry are sourced from RCSB PDB (https://www.rcsb.org).

(L.C.P.) for crystallisation [102,103] and the application of lipidic nanodiscs in solubilisation or reconstitution of isolated membrane protein complexes for cryo-EM specimen preparation [104,105] have shown superior stabilisation effect so as to improve resolution. This can be exemplified by the X-ray structure of *Thermus thermophillus* cyt caa_3 oxidase (2.36 Å resolution, L.C.P. [106]), cryo-EM structures of *Escherichia coli* cyt *bd* oxidase (2.68 Å resolution, nanodiscs [107]) and the cryo-EM structure of *Paracoccus denitrificans* cyt *c* oxidase (2.37 Å resolution, nanodiscs [108]; all resolution of cryo-EM data refer to the FSC = 0.143 criteria for the same basis of comparison). Respiratory chain complexes and supercomplexes in nanodiscs may provide additional information about partitioning of co-purified quinone molecules and their trajectories to fully reflect the native electron transport chain in the hydrophobic environment. Finally, structural studies using *in situ* cryogenic electron tomography (cryo-ET) permits the determination of higher order assemblies of protein complexes as well as structural dynamics directly in cells [109]. Although many technical limitations, such as to resolve small molecules with sufficient resolution still need to be overcome, the rapid and intensive development of cryo-ET [110] will eventually allow to visualise the respiratory chain and photosynthesis complexes in cellular context and maybe in action.

Perspectives

- Structural biology research of cyt *bc* complexes will contribute to an in-depth understanding of redox-driven proton translocation via the Q cycle and its regulation as well as support the design of fungicides, anti-malarial and anti-tuberculosis drugs.
- Structural characterisation of cyt *bc* complexes from a wide spectrum of species as well as in different types of supercomplexes is important to expand the knowledge on conserved and species-specific binding modes of native substrates, drugs, and inhibitors at the quinone binding sites.
- Structural information on the enzyme-substrate complex and defined catalytic states of cyt *bc* complexes is still lacking. We encourage that the cryo-EM specimens or crystals should be prepared in lipid environment.

Competing Interests

The authors declare that there are no competing interests associated with the manuscript.

Funding

This work was supported by the Deutsche Forschungsgemeinschaft (DFG, German Research Foundation) under Germany's Excellence Initiative (BIOSS — EXC-294) and Excellence Strategy (CIBSS — EXC-2189 — Project ID 390939984) in the form of project funding to C.H., by the DFG through Project-ID 403222702/SFB 1381 (C.H.).

Biochemical Society Transactions (2022) **50** 877–893
https://doi.org/10.1042/BST20190963

Author Contributions

W.-C.K. and C.H. conceived and wrote the paper.

Acknowledgements

We thank Christophe Wirth, Daniela Loher, Roshan Jha, and Claire Ortmann de Percin Northumberland for discussion.

Abbreviations

DMK, demethylmenaquinone; ETC, electron transport chain; ISP, iron-sulfur protein.

References

1 Kaila, V.R.I. and Wikström, M. (2021) Architecture of bacterial respiratory chains. *Nat. Rev. Microbiol.* **19**, 319–330 https://doi.org/10.1038/s41579-020-00486-4
2 Sarewicz, M., Pintscher, S., Pietras, R., Borek, A., Bujnowicz, Ł., Hanke, G. et al. (2021) Catalytic reactions and energy conservation in the cytochrome bc_1 and b_6f complexes of energy-transducing membranes. *Chem. Rev.* **121**, 2020–2108 https://doi.org/10.1021/acs.chemrev.0c00712
3 Vercellino, I. and Sazanov, L.A. (2021) The assembly, regulation and function of the mitochondrial respiratory chain. *Nat. Rev. Mol. Cell Biol.* **23**, 144–161 https://doi.org/10.1038/s41580-021-00415-0
4 Collins, M.D., Pirouz, T., Goodfellow, M. and Minnikin, D.E. (1977) Distribution of menaquinones in actinomycetes and corynebacteria. *Microbiology* **100**, 221–230 https://doi.org/10.1099/00221287-100-2-221
5 Collins, M.D. and Jones, D. (1981) Distribution of isoprenoid quinone structural types in bacteria and their taxonomic implication. *Microbiol. Rev.* **45**, 316–354 https://doi.org/10.1128/mr.45.2.316-354.1981
6 Rich, P.R. (2004) The quinone chemistry of *bc* complexes. *Biochim. Biophys. Acta* **1658**, 165–171 https://doi.org/10.1016/j.bbabio.2004.04.021
7 Crane, F.L. (2007) Discovery of ubiquinone (coenzyme Q) and an overview of function. *Mitochondrion* **7**, S2–S7 https://doi.org/10.1016/j.mito.2007.02.011
8 Crane, F.L. (2008) The evolution of coenzyme Q. *Biofactors* **32**, 5–11 https://doi.org/10.1002/biof.5520320102
9 Kurisu, G., Zhang, H., Smith, J.L. and Cramer, W.A. (2003) Structure of the cytochrome b_6f complex of oxygenic photosynthesis: tuning the cavity. *Science* **302**, 1009–1014 https://doi.org/10.1126/science.1090165
10 Stroebel, D., Choquet, Y., Popot, J.-L. and Picot, D. (2003) An atypical haem in the cytochrome b_6f complex. *Nature* **426**, 413–418 https://doi.org/10.1038/nature02155
11 Cramer, W.A. (2019) Structure–function of the cytochrome b_6f lipoprotein complex: a scientific odyssey and personal perspective. *Photosynth. Res.* **139**, 53–65 https://doi.org/10.1007/s11120-018-0585-x
12 Nelson, N. and Ben-Shem, A. (2004) The complex architecture of oxygenic photosynthesis. *Nat. Rev. Mol. Cell Biol* **5**, 971–982 https://doi.org/10.1038/nrm1525
13 Baymann, F., Schoepp-Cothenet, B., Lebrun, E., Rv, L. and Nitschke, W. (2012) Phylogeny of Rieske/cyt *b* complexes with a special focus on the haloarchaeal enzymes. *Genome Biol. Evol.* **4**, 832–841 https://doi.org/10.1093/gbe/evs056
14 Kao, W.-C. and Hunte, C. (2014) The molecular evolution of the Q_o motif. *Genome Biol. Evol.* **6**, 1894–1910 https://doi.org/10.1093/gbe/evu147
15 Iwata, S., Lee, J.W., Okada, K., Lee, J.K., Iwata, M., Rasmussen, B. et al. (1998) Complete structure of the 11-subunit bovine mitochondrial cytochrome bc_1 complex. *Science* **281**, 64–71 https://doi.org/10.1126/science.281.5373.64
16 Zhang, Z., Huang, L., Shulmeister, V.M., Chi, Y.-I., Kim, K.K., Hung, L.-W. et al. (1998) Electron transfer by domain movement in cytochrome bc_1. *Nature* **392**, 677–684 https://doi.org/10.1038/33612
17 Hunte, C., Koepke, J., Lange, C., Roßmanith, T. and Michel, H. (2000) Structure at 2.3 Å resolution of the cytochrome bc_1 complex from the yeast *saccharomyces cerevisiae* co-crystallized with an antibody Fv fragment. *Structure* **8**, 669–684 https://doi.org/10.1016/S0969-2126(00)00152-0
18 Kao, W.-C., Kleinschroth, T., Nitschke, W., Baymann, F., Neehaul, Y., Hellwig, P. et al. (2016) The obligate respiratory supercomplex from actinobacteria. *Biochim. Biophys. Acta* **1857**, 1705–1714 https://doi.org/10.1016/j.bbabio.2016.07.009
19 Kao, W.-C., Ortmann de Percin Northumberland, C., Cheng, T.C., Ortiz, J., Durand, A., von Loeffelholz, O. et al. (2022) Structural basis for safe and efficient energy conversion in a respiratory supercomplex. *Nat. Commun.* **13**, 545 https://doi.org/10.1038/s41467-022-28179-x
20 Crofts, A.R. (2004) The Q-cycle – a personal perspective. *Photosynth. Res.* **80**, 223–243 https://doi.org/10.1023/B:PRES.0000030444.52579.10
21 Crofts, A.R. (2004) The cytochrome bc_1 complex: function in the context of structure. *Annu. Rev. Physiol.* **66**, 689–733 https://doi.org/10.1146/annurev.physiol.66.032102.150251
22 Crofts, A.R. (2004) Proton-coupled electron transfer at the Q_o-site of the bc_1 complex controls the rate of ubihydroquinone oxidation. *Biochim. Biophys. Acta* **1655**, 77–92 https://doi.org/10.1016/j.bbabio.2003.10.012
23 Cramer, W.A., Hasan, S.S. and Yamashita, E. (2011) The Q cycle of cytochrome *bc* complexes: a structure perspective. *Biochim. Biophys. Acta* **1807**, 788–802 https://doi.org/10.1016/j.bbabio.2011.02.006
24 Crofts, A.R. (2021) The modified Q-cycle: a look back at its development and forward to a functional model. *Biochim. Biophys. Acta* **1862**, 148417 https://doi.org/10.1016/j.bbabio.2021.148417
25 Darrouzet, E., Valkova-Valchanova, M., Moser, C.C., Dutton, P.L. and Daldal, F. (2000) Uncovering the [2Fe2S] domain movement in cytochrome bc_1 and its implications for energy conversion. *Proc. Natl Acad. Sci. U.S.A.* **97**, 4567–4572 https://doi.org/10.1073/pnas.97.9.4567
26 Darrouzet, E., Moser, C.C., Dutton, P.L. and Daldal, F. (2001) Large scale domain movement in cytochrome bc_1: a new device for electron transfer in proteins. *Trends Biochem. Sci.* **26**, 445–451 https://doi.org/10.1016/S0968-0004(01)01897-7
27 Esser, L., Gong, X., Yang, S., Yu, L., Yu, C.-A. and Xia, D. (2006) Surface-modulated motion switch: capture and release of iron–sulfur protein in the cytochrome bc_1 complex. *Proc. Natl Acad. Sci. U.S.A.* **103**, 13045–13050 https://doi.org/10.1073/pnas.0601149103

28 Page, C.C., Moser, C.C., Chen, X. and Dutton, P.L. (1999) Natural engineering principles of electron tunnelling in biological oxidation–reduction. *Nature* **402**, 47–52 https://doi.org/10.1038/46972
29 Osyczka, A., Moser, C.C., Daldal, F. and Dutton, P.L. (2004) Reversible redox energy coupling in electron transfer chains. *Nature* **427**, 607–612 https://doi.org/10.1038/nature02242
30 Osyczka, A., Moser, C.C. and Dutton, P.L. (2005) Fixing the Q cycle. *Trends Biochem. Sci.* **30**, 176–182 https://doi.org/10.1016/j.tibs.2005.02.001
31 Crofts, A.R., Lhee, S., Crofts, S.B., Cheng, J. and Rose, S. (2006) Proton pumping in the bc_1 complex: a new gating mechanism that prevents short circuits. *Biochim. Biophys. Acta* **1757**, 1019–1034 https://doi.org/10.1016/j.bbabio.2006.02.009
32 Cape, J.L., Bowman, M.K. and Kramer, D.M. (2007) A semiquinone intermediate generated at the Q_o site of the cytochrome bc_1 complex: importance for the Q-cycle and superoxide production. *Proc. Natl Acad. Sci. U.S.A.* **104**, 7887–7892 https://doi.org/10.1073/pnas.0702621104
33 Pietras, R., Sarewicz, M. and Osyczka, A. (2016) Distinct properties of semiquinone species detected at the ubiquinol oxidation Q_o site of cytochrome bc_1 and their mechanistic implications. *J. R. Soc. Interface* **13**, 20160133 https://doi.org/10.1098/rsif.2016.0133
34 Sarewicz, M., Bujnowicz, Ł., Bhaduri, S., Singh, S.K., Cramer, W.A. and Osyczka, A. (2017) Metastable radical state, nonreactive with oxygen, is inherent to catalysis by respiratory and photosynthetic cytochromes bc_1/b_6f. *Proc. Natl Acad. Sci. U.S.A.* **114**, 1323–1328 https://doi.org/10.1073/pnas.1618840114
35 Saeb-Parsy, K., Martin, J.L., Summers, D.M., Watson, C.J.E., Krieg, T. and Murphy, M.P. (2021) Mitochondria as therapeutic targets in transplantation. *Trends Mol. Med.* **27**, 185–198 https://doi.org/10.1016/j.molmed.2020.08.001
36 Ishikita, H. and Saito, K. (2014) Proton transfer reactions and hydrogen-bond networks in protein environments. *J. R. Soc. Interface* **11**, 20130518 https://doi.org/10.1098/rsif.2013.0518
37 Esser, L., Quinn, B., Li, Y.-F., Zhang, M., Elberry, M., Yu, L. et al. (2004) Crystallographic studies of quinol oxidation site inhibitors: a modified classification of inhibitors for the cytochrome bc_1 complex. *J. Mol. Biol.* **341**, 281–302 https://doi.org/10.1016/j.jmb.2004.05.065
38 Huang, L.-S., Cobessi, D., Tung, E.Y. and Berry, E.A. (2005) Binding of the respiratory chain inhibitor antimycin to the mitochondrial bc_1 complex: a new crystal structure reveals an altered intramolecular hydrogen-bonding pattern. *J. Mol. Biol.* **351**, 573–597 https://doi.org/10.1016/j.jmb.2005.05.053
39 Hao, G.-F., Wang, F., Li, H., Zhu, X.-L., Yang, W.-C., Huang, L.-S. et al. (2012) Computational discovery of picomolar Q_o site inhibitors of cytochrome bc_1 complex. *J. Am. Chem. Soc.* **134**, 11168–11176 https://doi.org/10.1021/ja3001908
40 Di Trani, J.M., Liu, Z., Whitesell, L., Brzezinski, P., Cowen, L.E. and Rubinstein, J.L. (2021) Rieske head domain dynamics and indazole-derivative inhibition of *Candida albicans* complex III. *Structure* **30**, 129–138 https://doi.org/10.1016/j.str.2021.08.006
41 Gu, J., Wu, M., Guo, R., Yan, K., Lei, J., Gao, N. et al. (2016) The architecture of the mammalian respirasome. *Nature* **537**, 639–643 https://doi.org/10.1038/nature19359
42 Letts, J.A., Fiedorczuk, K. and Sazanov, L.A. (2016) The architecture of respiratory supercomplexes. *Nature* **537**, 644–648 https://doi.org/10.1038/nature19774
43 Wu, M., Gu, J., Guo, R., Huang, Y. and Yang, M. (2016) Structure of mammalian respiratory supercomplex $I_1III_2IV_1$. *Cell* **167**, 1598–1609.e10 https://doi.org/10.1016/j.cell.2016.11.012
44 Guo, R., Zong, S., Wu, M., Gu, J. and Yang, M. (2017) Architecture of human mitochondrial respiratory megacomplex $I_2III_2IV_2$. *Cell* **170**, 1247–1257.e12 https://doi.org/10.1016/j.cell.2017.07.050
45 Davies, K.M., Blum, T.B. and Kühlbrandt, W. (2018) Conserved in situ arrangement of complex I and III_2 in mitochondrial respiratory chain supercomplexes of mammals, yeast, and plants. *Proc. Natl Acad. Sci. U.S.A.* **115**, 3024–3029 https://doi.org/10.1073/pnas.1720702115
46 Hartley, A.M., Lukoyanova, N., Zhang, Y., Cabrera-Orefice, A., Arnold, S., Meunier, B. et al. (2018) Structure of yeast cytochrome *c* oxidase in a supercomplex with cytochrome bc_1. *Nat. Struct. Mol. Biol.* **26**, 78–83 https://doi.org/10.1038/s41594-018-0172-z
47 Rathore, S., Berndtsson, J., Marin-Buera, L., Conrad, J., Carroni, M., Brzezinski, P. et al. (2018) Cryo-EM structure of the yeast respiratory supercomplex. *Nat. Struct. Mol. Biol.* **26**, 50–57 https://doi.org/10.1038/s41594-018-0169-7
48 Letts, J.A., Fiedorczuk, K., Degliesposti, G., Skehel, M. and Sazanov, L.A. (2019) Structures of respiratory supercomplex I+III_2 reveal functional and conformational crosstalk. *Mol. Cell* **75**, 1131–1146 https://doi.org/10.1016/j.molcel.2019.07.022
49 Berry, E.A., Huang, L.-S., Saechao, L.K., Pon, N.G., Valkova-Valchanova, M. and Daldal, F. (2004) X-ray structure of *Rhodobacter capsulatus* cytochrome bc_1: comparison with its mitochondrial and chloroplast counterparts. *Photosynth. Res.* **81**, 251–275 https://doi.org/10.1023/B:PRES.0000036888.18223.0e
50 Kleinschroth, T., Castellani, M., Trinh, C.H., Morgner, N., Brutschy, B., Ludwig, B. et al. (2011) X-ray structure of the dimeric cytochrome bc_1 complex from the soil bacterium *Paracoccus denitrificans* at 2.7-Å resolution. *Biochim. Biophys. Acta* **1807**, 1606–1615 https://doi.org/10.1016/j.bbabio.2011.09.017
51 Malone, L.A., Qian, P., Mayneord, G.E., Hitchcock, A., Farmer, D.A., Thompson, R.F. et al. (2019) Cryo-EM structure of the spinach cytochrome b_6f complex at 3.6 Å resolution. *Nature* **575**, 535–539 https://doi.org/10.1038/s41586-019-1746-6
52 Gong, H., Li, J., Xu, A., Tang, Y., Ji, W., Gao, R. et al. (2018) An electron transfer path connects subunits of a mycobacterial respiratory supercomplex. *Science* **362**, eaat8923 https://doi.org/10.1126/science.aat8923
53 Wiseman, B., Nitharwal, R.G., Fedotovskaya, O., Schäfer, J., Guo, H., Kuang, Q. et al. (2018) Structure of a functional obligate complex III_2IV_2 respiratory supercomplex from *mycobacterium smegmatis*. *Nat. Struct. Mol. Biol.* **25**, 1128–1136 https://doi.org/10.1038/s41594-018-0160-3
54 Moe, A., Kovalova, T., Król, S., Yanofsky, D.J., Bott, M., Sjöstrand, D. et al. (2021) The respiratory supercomplex from *C. glutamicum*. *Structure* **30**, 338–349 https://doi.org/10.1016/j.str.2021.11.008
55 Schütz, M., Brugna, M., Lebrun, E., Baymann, F., Huber, R., Stetter, K.-O. et al. (2000) Early evolution of cytochrome *bc* complexes. *J. Mol. Biol.* **300**, 663–675 https://doi.org/10.1006/jmbi.2000.3915
56 Schoepp-Cothenet, B., Lieutaud, C., Baymann, F., Verméglio, A., Friedrich, T., Kramer, D.M. et al. (2009) Menaquinone as pool quinone in a purple bacterium. *Proc. Natl Acad. Sci. U.S.A.* **106**, 8549–8554 https://doi.org/10.1073/pnas.0813173106
57 Bergdoll, L., ten Brink, F., Nitschke, W., Picot, D. and Baymann, F. (2016) From low- to high-potential bioenergetic chains: thermodynamic constraints of Q-cycle function. *Biochim. Biophys. Acta* **1857**, 1569–1579 https://doi.org/10.1016/j.bbabio.2016.06.006
58 von Jagow, G. and Link, T.A. (1986) [24] Use of specific inhibitors on the mitochondrial bc_1 complex. *Methods Enzymol.* **126**, 253–271 https://doi.org/10.1016/S0076-6879(86)26026-7

59 Palsdóttir, H., Lojero, C.G., Trumpower, B.L. and Hunte, C. (2003) Structure of the yeast cytochrome bc_1 complex with a hydroxyquinone anion Q_o site inhibitor bound. *J. Biol. Chem.* **278**, 31303–31311 https://doi.org/10.1074/jbc.M302195200

60 Crofts, A.R., Hong, S., Wilson, C., Burton, R., Victoria, D., Harrison, C. et al. (2013) The mechanism of ubihydroquinone oxidation at the Q_o-site of the cytochrome bc_1 complex. *Biochim. Biophys. Acta* **1827**, 1362–1377 https://doi.org/10.1016/j.bbabio.2013.01.009

61 Wilson, C.A. and Crofts, A.R. (2018) Dissecting the pattern of proton release from partial process involved in ubihydroquinone oxidation in the Q-cycle. *Biochim. Biophys. Acta* **1859**, 531–543 https://doi.org/10.1016/j.bbabio.2018.03.016

62 Link, T.A. (1997) The role of the 'Rieske' iron sulfur protein in the hydroquinone oxidation Q_p site of the cytochrome bc_1 complex. The 'proton-gated affinity change' mechanism. *FEBS Lett.* **412**, 257–264 https://doi.org/10.1016/S0014-5793(97)00772-2

63 Zu, Y., Couture, M.M.J., Kolling, D.R.J., Crofts, A.R., Eltis, L.D., Fee, J.A. et al. (2003) Reduction potentials of Rieske clusters: importance of the coupling between oxidation state and histidine protonation state. *Biochemistry* **42**, 12400–12408 https://doi.org/10.1021/bi0350957

64 Yanofsky, D.J., Di Trani, J.M., Krol, S., Abdelaziz, R., Bueler, S.A., Imming, P. et al. (2021) Structure of mycobacterial $CIII_2CIV_2$ respiratory supercomplex bound to the tuberculosis drug candidate telacebec (Q203). *eLife* **10**, e71959 https://doi.org/10.7554/eLife.71959

65 Zhou, S., Wang, W., Zhou, X., Zhang, Y., Lai, Y., Tang, Y. et al. (2021) Structure of *Mycobacterium tuberculosis* cytochrome *bcc* in complex with Q203 and TB47, two anti-TB drug candidates. *eLife* **10**, e69418 https://doi.org/10.7554/eLife.69418

66 Lancaster, C.R.D. and Michel, H. (1997) The coupling of light-induced electron transfer and proton uptake as derived from crystal structures of reaction centres from *Rhodopseudomonas viridis* modified at the binding site of the secondary quinone, Q_B. *Structure* **5**, 1339–1359 https://doi.org/10.1016/S0969-2126(97)00285-2

67 Lancaster, C.R.D., Hunte, C., Kelley, J., Trumpower, B.L. and Ditchfield, R. (2007) A comparison of stigmatellin conformations, free and bound to the photosynthetic reaction center and the cytochrome bc_1 complex. *J. Mol. Biol.* **368**, 197–208 https://doi.org/10.1016/j.jmb.2007.02.013

68 Berry, E.A., Huang, L.-S., Lee, D.-W., Daldal, F., Nagai, K. and Minagawa, N. (2010) Ascochlorin is a novel, specific inhibitor of the mitochondrial cytochrome bc_1 complex. *Biochim. Biophys. Acta* **1797**, 360–370 https://doi.org/10.1016/j.bbabio.2009.12.003

69 Esser, L., Elberry, M., Zhou, F., Yu, C.-A., Yu, L. and Xia, D. (2008) Inhibitor-complexed structures of the cytochrome bc_1 from the photosynthetic bacterium *Rhodobacter sphaeroides*. *J. Biol. Chem.* **283**, 2846–2857 https://doi.org/10.1074/jbc.M708608200

70 Holländer, R. (1976) Correlation of the function of demethylmenaquinone in bacterial electron transport with its redox potential. *FEBS Lett.* **72**, 98–100 https://doi.org/10.1016/0014-5793(76)80821-6

71 Schütz, M., Schoepp-Cothenet, B., Lojou, E., Woodstra, M., Lexa, D., Tron, P. et al. (2003) The naphthoquinol oxidizing cytochrome bc_1 complex of the hyperthermophilic Knallgasbacterium *Aquifex aeolicus*: properties and phylogenetic relationships. *Biochemistry* **42**, 10800–10808 https://doi.org/10.1021/bi034452a

72 Zhu, G., Zeng, H., Zhang, S., Juli, J., Pang, X., Hoffmann, J. et al. (2020) A 3.3 Å-resolution structure of hyperthermophilic respiratory complex III reveals the mechanism of its thermal stability. *Angew. Chem. Int. Ed. Engl.* **59**, 343–351 https://doi.org/10.1002/anie.201911554

73 Esser, L., Zhou, F., Yu, C.-A. and Xia, D. (2019) Crystal structure of bacterial cytochrome bc_1 in complex with azoxystrobin reveals a conformational switch of the Rieske iron–sulfur protein subunit. *J. Biol. Chem.* **294**, 12007–12019 https://doi.org/10.1074/jbc.RA119.008381

74 Sauter, H., Steglich, W. and Anke, T. (1999) Strobilurins: evolution of a new class of active substances. *Angew. Chem. Int. Ed. Engl.* **38**, 1328–1349 https://doi.org/10.1002/(SICI)1521-3773(19990517)38:10<1328::AID-ANIE1328>3.0.CO;2-1

75 Bartlett, D.W., Clough, J.M., Godwin, J.R., Hall, A.A., Hamer, M. and Parr-Dobrzanski, B. (2002) The strobilurin fungicides. *Pest. Manag. Sci.* **58**, 649–662 https://doi.org/10.1002/ps.520

76 Casida, J.E. and Durkin, K.A. (2017) Pesticide chemical research in toxicology: lessons from nature. *Chem. Res. Toxicol.* **30**, 94–104 https://doi.org/10.1021/acs.chemrestox.6b00303

77 Gao, X., Wen, X., Yu, C., Esser, L., Tsao, S., Quinn, B. et al. (2002) The crystal structure of mitochondrial cytochrome bc_1 in complex with famoxadone: the role of aromatic–aromatic interaction in inhibition. *Biochemistry* **41**, 11692–11702 https://doi.org/10.1021/bi026252p

78 Birth, D., Kao, W.-C. and Hunte, C. (2014) Structural analysis of atovaquone-inhibited cytochrome bc_1 complex reveals the molecular basis of antimalarial drug action. *Nat. Commun.* **5**, 4029 https://doi.org/10.1038/ncomms5029

79 Painter, H.J., Morrisey, J.M., Mather, M.W. and Vaidya, A.B. (2007) Specific role of mitochondrial electron transport in blood-stage *Plasmodium falciparum*. *Nature* **446**, 88–91 https://doi.org/10.1038/nature05572

80 Barton, V., Fisher, N., Biagini, G.A., Ward, S.A. and O'Neill, P.M. (2010) Inhibiting *Plasmodium* cytochrome bc_1: a complex issue. *Curr. Opin. Chem. Biol.* **14**, 440–446 https://doi.org/10.1016/j.cbpa.2010.05.005

81 Fisher, N., Meunier, B. and Biagini, G.A. (2020) The cytochrome bc_1 complex as an antipathogenic target. *FEBS Lett.* **594**, 2935–2952 https://doi.org/10.1002/1873-3468.13868

82 Argy, N., Gal, S.L., Coppée, R., Song, Z., Vindrios, W., Massias, L. et al. (2018) *Pneumocystis* cytochrome *b* mutants associated with atovaquone prophylaxis failure as the cause of *Pneumocystis* infection outbreak among heart transplant recipients. *Clin. Infect. Dis.* **67**, 913–919 https://doi.org/10.1093/cid/ciy154

83 Fisher, N. and Meunier, B. (2008) Molecular basis of resistance to cytochrome bc_1 inhibitors. *FEMS Yeast Res.* **8**, 183–192 https://doi.org/10.1111/j.1567-1364.2007.00328.x

84 Biagini, G.A., Fisher, N., Shone, A.E., Mubaraki, M.A., Srivastava, A., Hill, A. et al. (2012) Generation of quinolone antimalarials targeting the *Plasmodium falciparum* mitochondrial respiratory chain for the treatment and prophylaxis of malaria. *Proc. Natl Acad. Sci. U.S.A.* **109**, 8298–8303 https://doi.org/10.1073/pnas.1205651109

85 Mounkoro, P., Michel, T., Benhachemi, R., Surpateanu, G., Iorga, B.I., Fisher, N. et al. (2019) Mitochondrial complex III Q_i-site inhibitor resistance mutations found in laboratory selected mutants and field isolates. *Pest. Manag. Sci.* **75**, 2107–2114 https://doi.org/10.1002/ps.5264

86 Dreinert, A., Wolf, A., Mentzel, T., Meunier, B. and Fehr, M. (2018) The cytochrome bc_1 complex inhibitor Ametoctradin has an unusual binding mode. *Biochim. Biophys. Acta* **1859**, 567–576 https://doi.org/10.1016/j.bbabio.2018.04.008

87 Song, Z., Iorga, B.I., Mounkoro, P., Fisher, N. and Meunier, B. (2018) The antimalarial compound ELQ-400 is an unusual inhibitor of the bc_1 complex, targeting both Q_o and Q_i sites. *FEBS Lett.* **592**, 1346–1356 https://doi.org/10.1002/1873-3468.13035

88 Capper, M.J., O'Neill, P.M., Fisher, N., Strange, R.W., Moss, D., Ward, S.A. et al. (2015) Antimalarial 4(1H)-pyridones bind to the Q_i site of cytochrome bc_1. *Proc. Natl Acad. Sci. U.S.A.* **112**, 755–760 https://doi.org/10.1073/pnas.1416611112

89 McPhillie, M., Zhou, Y., Bissati, K.E., Dubey, J., Lorenzi, H., Capper, M. et al. (2016) New paradigms for understanding and step changes in treating active and chronic, persistent apicomplexan infections. *Sci. Rep.* **6**, 29179 https://doi.org/10.1038/srep29179
90 Hong, W.D., Leung, S.C., Amporndanai, K., Davies, J., Priestley, R.S., Nixon, G.L. et al. (2018) Potent antimalarial 2-pyrazolyl quinolone bc_1 Q_i inhibitors with improved drug-like properties. *ACS Med. Chem. Lett.* **9**, 1205–1210 https://doi.org/10.1021/acsmedchemlett.8b00371
91 Amporndanai, K., Johnson, R.M., O'Neill, P.M., Fishwick, C.W.G., Jamson, A.H., Rawson, S. et al. (2018) X-ray and cryo-EM structures of inhibitor-bound cytochrome bc_1 complexes for structure-based drug discovery. *IUCrJ* **5**, 200–210 https://doi.org/10.1107/S2052252518001616
92 Pethe, K., Bifani, P., Jang, J., Kang, S., Park, S., Ahn, S. et al. (2013) Discovery of Q203, a potent clinical candidate for the treatment of tuberculosis. *Nat. Med.* **19**, 1157–1160 https://doi.org/10.1038/nm.3262
93 Falcon, B., Zivanov, J., Zhang, W., Murzin, A.G., Garringer, H.J., Vidal, R. et al. (2019) Novel tau filament fold in chronic traumatic encephalopathy encloses hydrophobic molecules. *Nature* **568**, 420–423 https://doi.org/10.1038/s41586-019-1026-5
94 Ho, C.-M., Li, X., Lai, M., Terwilliger, T.C., Beck, J.R., Wohlschlegel, J. et al. (2019) Bottom-up structural proteomics: cryoEM of protein complexes enriched from the cellular milieu. *Nat. Methods* **17**, 79–85 https://doi.org/10.1038/s41592-019-0637-y
95 Rawson, S., McPhillie, M.J., Johnson, R.M., Fishwick, C.W.G. and Muench, S.P. (2017) The potential use of single-particle electron microscopy as a tool for structure-based inhibitor design. *Acta Crystallogr. D. Biol. Crystallogr.* **73**, 534–540 https://doi.org/10.1107/S2059798317004077
96 Renaud, J.-P., Chari, A., Ciferri, C., Liu, W.T., Rémigy, H.-W., Stark, H. et al. (2018) Cryo-EM in drug discovery: achievements, limitations and prospects. *Nat. Rev. Drug Discov.* **17**, 471–492 https://doi.org/10.1038/nrd.2018.77
97 Ceska, T., Chung, C.-W., Cooke, R., Phillips, C. and Williams, P.A. (2019) Cryo-EM in drug discovery. *Biochem. Soc. Trans.* **47**, 281–293 https://doi.org/10.1042/BST20180267
98 García-Nafría, J. and Tate, C.G. (2020) Cryo-electron microscopy: moving beyond X-ray crystal structures for drug receptors and drug development. *Annu. Rev. Pharmacol. Toxicol.* **60**, 1–21 https://doi.org/10.1146/annurev-pharmtox-010919-023545
99 Hunte, C. and Richers, S. (2008) Lipids and membrane protein structures. *Curr. Opin. Struc. Biol.* **18**, 406–411 https://doi.org/10.1016/j.sbi.2008.03.008
100 Birch, J., Axford, D., Foadi, J., Meyer, A., Eckhardt, A., Thielmann, Y. et al. (2018) The fine art of integral membrane protein crystallisation. *Methods* **147**, 150–162 https://doi.org/10.1016/j.ymeth.2018.05.014
101 Sgro, G.G. and Costa, T.R.D. (2018) Cryo-EM grid preparation of membrane protein samples for single particle analysis. *Front. Mol. Biosci.* **5**, 74 https://doi.org/10.3389/fmolb.2018.00074
102 Ma, P., Weichert, D., Aleksandrov, L.A., Jensen, T.J., Riordan, J.R., Liu, X. et al. (2017) The cubicon method for concentrating membrane proteins in the cubic mesophase. *Nat. Protoc.* **12**, 1745–1762 https://doi.org/10.1038/nprot.2017.057
103 Broecker, J., Morizumi, T., Ou, W.-L., Klingel, V., Kuo, A., Kissick, D.J. et al. (2018) High-throughput in situ X-ray screening of and data collection from protein crystals at room temperature and under cryogenic conditions. *Nat. Protoc.* **13**, 260–292 https://doi.org/10.1038/nprot.2017.135
104 Sun, C. and Gennis, R.B. (2019) Single-particle cryo-EM studies of transmembrane proteins in SMA copolymer nanodiscs. *Chem. Phys. Lipids* **221**, 114–119 https://doi.org/10.1016/j.chemphyslip.2019.03.007
105 Hesketh, S.J., Klebl, D.P., Higgins, A.J., Thomsen, M., Pickles, I.B., Sobott, F. et al. (2020) Styrene maleic-acid lipid particles (SMALPs) into detergent or amphipols: an exchange protocol for membrane protein characterisation. *Biochim. Biophys. Acta* **1862**, 183192 https://doi.org/10.1016/j.bbamem.2020.183192
106 Lyons, J.A., Aragão, D., Slattery, O., Pisliakov, A.V., Soulimane, T. and Caffrey, M. (2012) Structural insights into electron transfer in caa_3-type cytochrome oxidase. *Nature* **487**, 514–518 https://doi.org/10.1038/nature11182
107 Safarian, S., Hahn, A., Mills, D.J., Radloff, M., Eisinger, M.L., Nikolaev, A. et al. (2019) Active site rearrangement and structural divergence in prokaryotic respiratory oxidases. *Science* **366**, 100–104 https://doi.org/10.1126/science.aay0967
108 Kolbe, F., Safarian, S., Piórek, Ż, Welsch, S., Müller, H. and Michel, H. (2021) Cryo-EM structures of intermediates suggest an alternative catalytic reaction cycle for cytochrome *c* oxidase. *Nat. Commun.* **12**, 6903 https://doi.org/10.1038/s41467-021-27174-y
109 Turk, M. and Baumeister, W. (2020) The promise and the challenges of cryo-electron tomography. *FEBS Lett.* **594**, 3243–3261 https://doi.org/10.1002/1873-3468.13948
110 Bäuerlein, F.J.B. and Baumeister, W. (2021) Towards visual proteomics at high resolution. *J. Mol. Biol.* **433**, 167187 https://doi.org/10.1016/j.jmb.2021.167187
111 Świerczek, M., Cieluch, E., Sarewicz, M., Borek, A., Moser, C.C., Dutton, P.L. et al. (2010) An electronic bus bar lies in the core of cytochrome bc_1. *Science* **329**, 451–454 https://doi.org/10.1126/science.1190899
112 Emsley, P., Lohkamp, B., Scott, W.G. and Cowtan, K. (2010) Features and development of Coot. *Acta Crystallogr. D. Biol. Crystallogr.* **66**, 486–501 https://doi.org/10.1107/S0907444910007493